

Characterizing the Impact of Feedback Delays on Wideband Rate Adaptation

Jobin Francis and Neelesh B. Mehta, *Senior Member, IEEE*

Abstract—In contemporary orthogonal frequency division multiplexing (OFDM) systems, such as Long Term Evolution (LTE), LTE-Advanced, and WiMAX, a codeword is transmitted over a group of subcarriers. Since different subcarriers see different channel gains in frequency-selective channels, the modulation and coding scheme (MCS) of the codeword must be selected based on the vector of signal-to-noise-ratios (SNRs) of these subcarriers. Exponential effective SNR mapping (EESM) maps the vector of SNRs into an equivalent flat-fading SNR, and is widely used to simplify this problem. We develop a new analytical framework to characterize the throughput of EESM-based rate adaptation in such wideband channels in the presence of feedback delays. We derive a novel accurate approximation for the throughput as a function of feedback delay. We also propose a novel bivariate gamma distribution to model the time evolution of EESM between the times of estimation and data transmission, which facilitates the analysis. These are then generalized to a multi-cell, multi-user scenario with various frequency-domain schedulers. Unlike prior work, most of which is simulation-based, our framework encompasses both correlated and independent subcarriers and various multiple antenna diversity modes; it is accurate over a wide range of delays.

Index Terms—OFDM, adaptation, Exponential Effective SNR Mapping (EESM), feedback delay, scheduling, co-channel interference, bivariate gamma distribution.

I. INTRODUCTION

CURRENT and next generation wireless systems, such as Long Term Evolution (LTE), LTE-Advanced, and WiMAX, have been designed to meet the incessant demand for higher data rates. They employ orthogonal frequency division multiplexing (OFDM) because it avoids inter-symbol and intra-cell interference. OFDM divides the available bandwidth into narrowband orthogonal subcarriers. To efficiently utilize the scarce bandwidth, adaptive modulation and coding (AMC), in which rate is adapted, and scheduling, in which the user that is transmitted to is adapted, are extensively utilized.

In these OFDM systems, a codeword is transmitted over a group of subcarriers [2]. Due to the frequency-selective nature of the channel, different subcarriers see different gains. Thus, the block error rate (BLER) is a function of the vector of

signal-to-noise-ratios (SNRs) of the subcarriers assigned to the codeword. Consequently, the AMC scheme must select the modulation and coding scheme (MCS) based on this vector of SNRs. Further, no closed-form expression for the BLER in vector channels is available. This is unlike the well-studied problem of AMC over narrowband channels, in which the MCS choice is based on just one SNR [3].

An important practical issue in these systems is the delay between the time of estimation of the channel gains and the time of data transmission. This delay ranges from milliseconds to tens of milliseconds [2]. It degrades the throughput because either the AMC scheme may overestimate or underestimate the rate or a sub-optimal user may get scheduled. Characterizing the effect of feedback delay on AMC over wideband channels is the focus of this paper.

AMC over frequency-selective fading channels, in principle, requires a cumbersome multi-dimensional lookup table to map the vector of SNRs to the MCS. Hence, link quality metrics (LQMs) such as exponential effective SNR mapping (EESM) have been developed to simplify this problem [4]–[6]. EESM maps the vector of subcarrier SNRs seen by the codeword into an effective flat-fading SNR, which is interpreted to be the equivalent SNR in an additive white Gaussian noise (AWGN) channel for that MCS. Thus, EESM reduces the problem of AMC over a frequency-selective channel to that over a frequency-flat channel. If $\gamma_i(t)$ denotes the SNR of the i th subcarrier at time t , for $1 \leq i \leq N_{sc}$, then the effective SNR $\gamma_{\text{eff}}^{(m)}(t)$ for MCS m is defined as

$$\gamma_{\text{eff}}^{(m)}(t) = -\beta_m \log \left(\frac{1}{N_{sc}} \sum_{i=1}^{N_{sc}} \exp \left(-\frac{\gamma_i(t)}{\beta_m} \right) \right), \quad (1)$$

where $\beta_m > 0$ is an MCS-dependent scaling parameter. Its accuracy has been conclusively established in several prior works [5], [6]. It has been widely used in system-level simulations of LTE and WiMAX [7], [8] and to generate feedback to the base station (BS) [9].

A. Related Literature

We first survey the simpler problem of characterizing the effect of feedback delay in narrowband systems, which has been widely studied in the literature. The effect of channel estimation errors, feedback errors, and feedback delay on throughput is analyzed in [10] for a single cell, multi-user system with a greedy scheduler. However, subcarrier-level scheduling and adaptation is assumed. Thus, the techniques for adaptation

Manuscript received April 15, 2014; revised August 16, 2014; accepted October 4, 2014. Date of publication October 15, 2014; date of current version February 6, 2015. This research is partially supported by a philanthropic grant from the Broadcom Foundation, USA. The associate editor coordinating the review of this paper and approving it for publication was L. Lai.

The authors are with the Department of Electrical Communication Engineering, Indian Institute of Science (IISc), Bangalore 560 012, India (e-mail: jobin@ece.iisc.ernet.in; nbmehta@ece.iisc.ernet.in).

Digital Object Identifier 10.1109/TWC.2014.2363083

over narrowband fading channels apply here. Subcarrier-level adaptation with feedback delays is also investigated in [11] for a point-to-point, single user scenario and in [12] for a multi-user, single cell scenario. In [13], the throughput of an OFDM system with various feedback reduction schemes, frequency-domain scheduling, and feedback delay is analyzed. A heterogeneous feedback scheme with imperfect channel state information is analyzed in [14]. However, both [13] and [14] use the narrowband rate adaptation model. The impact of feedback delays on transmit beamforming in a fixed rate, narrowband system is studied in [15].

As mentioned before, rate adaptation in wideband channels is much more involved, and LQMs enable it to be systematically implemented and investigated. LQM-based link adaptation without feedback delays is studied in [16], [17] and with feedback delays in [4]. However, only Monte Carlo simulation results are presented in [4], [16], [17]. The impact of the coarseness of the channel quality feedback on the downlink throughput of LTE is analyzed in [9]. In it, EESM-based feedback is used. However, feedback delays are ignored. The throughput of EESM-based AMC is analyzed in [18] for a point-to-point system as well as for a multi-user, multi-cell system with frequency-domain scheduling. Here again, feedback delay is not considered.

B. Contributions

From the survey above, we see that the effect of feedback delay for the practically important case in which a codeword, whose MCS is adapted, is transmitted over multiple subcarriers that see different, albeit correlated, gains has not been analyzed. We address this by developing a novel, comprehensive analytical framework for the throughput of EESM-based AMC with feedback delays.

We first consider the problem of wideband adaptation in a point-to-point link with fading. A new challenge that we have to address here is that with feedback delays, the joint or bivariate distribution of the effective SNRs $\gamma_{\text{eff}}^{(m_1)}(t)$ and $\gamma_{\text{eff}}^{(m_2)}(t + \tau)$, each of which is a non-linear mapping of subcarrier SNRs, is needed. This is because the MCS m_1 is decided at time t on the basis of $\gamma_{\text{eff}}^{(1)}(t), \dots, \gamma_{\text{eff}}^{(L)}(t)$, where L is the number of MCSs available to choose from, while the success of the transmission depends on $\gamma_{\text{eff}}^{(m_1)}(t + \tau)$.

We propose modeling the joint distribution of the random variables (RVs) $\gamma_{\text{eff}}^{(m)}(t)$ and $\gamma_{\text{eff}}^{(m)}(t + \tau)$ with a bivariate gamma probability density function (PDF) [19]. To the best of our knowledge, this is the first bivariate statistical characterization of the time evolution of EESM. The choice of the distribution is motivated by the fact that at high correlations, in which the subcarrier gains are almost the same, it can be seen from (1) that $\gamma_{\text{eff}}^{(m)}(t) \approx \gamma_i(t)$, for any $1 \leq i \leq N_{\text{sc}}$, at any time t . However, as we shall see, the bivariate gamma distribution is quite accurate even for the other extreme case of independent subcarriers. We note that this is not a simple extension of [18], [20] because no tractable, natural extension to the bivariate case exists in the literature for the beta model of [18], and the generalized extreme value (GEV) and Pearson models of [20].

While the lognormal model proposed in [9] can be extended, we shall see that it is inaccurate.

We propose a new moment generating function (MGF)-matching method [21] that is uniquely well-suited to EESM to determine the parameters of the bivariate gamma distribution. The proposed model is then used to obtain a novel expression for the throughput with feedback delays. Our analysis covers multiple antenna modes, it accounts for any general model for correlation among the subcarriers, and is accurate.

We then generalize the model to analyze the downlink throughput of a cellular system that consists of multiple cells with multiple users per cell, uses frequency-domain scheduling, faces feedback delays and co-channel interference, and in which the links undergo both shadowing and fading. Here, due to shadowing and interference, the subcarrier signal-to-interference-plus-noise-ratios (SINRs) are no longer gamma distributed. Therefore, we present a novel bivariate gamma mixture model, which generalizes the above bivariate gamma model. We then derive novel expressions for the cell throughput with round robin (RR), greedy, and modified proportional fair (MPF) schedulers, which cover a wide range of the throughput versus fairness trade-off [10], [13], [22].

We note that this paper makes several advances over [9], [18], which do not model feedback delays. As we saw above, the introduction of feedback delays is not a simple extension because it begets a much more challenging and involved analysis, and leads to a different expression for the throughput. We also note that both bivariate and bivariate mixture models developed in this paper are significant extensions of the models developed in [9] and [18]. Further, [9] assumes the same value of β_m for all the MCSs. However, for LTE, this assumption breaks down because β_m varies over a wide range of values from 1.0 for QPSK with rate 0.08 code to 28.9 for 64-QAM with rate 0.93 code [23]. We do not make this assumption. Consequently, in our model for wideband rate adaptation, even with EESM the MCS has to be decided based on multiple effective SNRs, one for each MCS. Another challenge is that these are correlated RVs since they are obtained from the same vector of subcarrier SNRs. When combined with feedback delays, it leads to an analysis that is different from that in [18]. Our multi-cell, multi-user model and analysis deviates from [18] even further as it requires the adoption of a novel and more general bivariate gamma mixture model.

C. Organization and Notation

The paper is organized as follows. Section II studies the point-to-point OFDM link with fading. The multi-cell, multi-user system with different schedulers is analyzed in Section III. Simulation results are presented in Section IV, and are followed by our conclusions in Section V.

We denote the transpose of a matrix \mathbf{A} by \mathbf{A}^T . For a complex number c , c^* and $|c|$ denote its complex conjugate and absolute value, respectively. $\mathbb{E}[X]$, $F_X(x)$, and $f_X(x)$ denote expectation, cumulative distribution function (CDF), and PDF, respectively of the RV X . The MGF $\Psi_X(z)$ of X is defined as $\mathbb{E}[\exp(-zX)]$. For two RVs X and Y , the conditional PDF

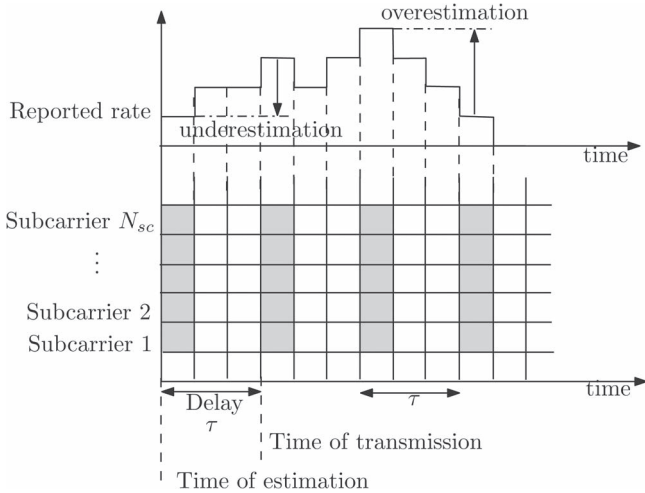


Fig. 1. System model for a point-to-point OFDM link with fading that shows the underestimation and overestimation of MCSs due to feedback delay.

of Y given $X = x$ is denoted by $f_Y(y|x)$. The joint MGF $\Psi_{X,Y}(z_1, z_2)$ is defined as $\mathbb{E}[\exp(-z_1X - z_2Y)]$.

II. POINT-TO-POINT LINK WITH FADING

We first consider a point-to-point OFDM link with N_t transmit antennas, N_r receive antennas, and frequency-selective fading. This is shown in Fig. 1. The transmitted codeword is encoded across N_{sc} subcarriers. Based on the channel gains of these subcarriers, the receiver selects an MCS and feeds it back to the transmitter. For example, in LTE, one among 16 different MCSs is fed back [2].

A. Channel Model

Let $h_{kl}^{(i)}(t)$ denote the complex channel gain between the k th receive antenna and the l th transmit antenna of the i th subcarrier at time t . It is a circularly symmetric complex Gaussian RV with unit variance. For the general uncorrelated scatterers assumption [3], which motivates most channel models considered in the literature, it can be shown that the channel gains of different subcarriers in an OFDM system are statistically identical [3], [24]. The correlation between the subcarriers depends on the *multipath delay spread* of the channel. Let τ denote the delay between the times of channel estimation and data transmission. Then, as per the Jakes' fading model [3], $h_{kl}^{(i)}(t)$ and $h_{kl}^{(i)}(t + \tau)$ are jointly Gaussian with correlation coefficient $\rho(\tau) = J_0(2\pi f_d \tau)$, where f_d is the Doppler spread and $J_0(\cdot)$ is the zeroth-order Bessel function of the first kind [25]. We shall refer to $f_d \tau$ as the *normalized delay*. To focus on the effect of feedback delays, the channel estimates at the receiver are assumed to be perfect, as has also been assumed in [4], [16], [17].

The complex channel gains on different transmit-receive (Tx-Rx) antenna pairs are assumed to be identically and independently distributed [3], [15], [24]. This is justified in a rich scattering environment when the antennas are co-located, yet spaced sufficiently far apart [3], [24]. Thus, the channel gain vector of the (k, l) th antenna pair at time t ,

$\mathbf{h}_{kl}(t) = [h_{kl}^{(1)}(t), h_{kl}^{(2)}(t), \dots, h_{kl}^{(N_{sc})}(t)]^T$ is a circularly symmetric complex Gaussian random vector with covariance matrix \mathbf{C} . Its (i, j) th element is $C_{ij} = \mathbb{E}[h_{kl}^{(i)}(t)h_{kl}^{(j)*}(t)]$.

Let σ^2 denote the average SNR of a Tx-Rx link. The subcarrier SNR $\gamma_i(t)$ depends on the multiple antenna mode used.¹ For single-input-single-output (SISO), i.e., $N_t = N_r = 1$, it is $\gamma_i(t) = \sigma^2 |h_{11}^{(i)}(t)|^2$. For single-input-multiple-output (SIMO) with $N_t = 1$, $N_r > 1$ and maximal ratio combining, it is $\gamma_i(t) = \sigma^2 \sum_{k=1}^{N_r} |h_{k1}^{(i)}(t)|^2$. Similarly, for multiple-input-single-output (MISO) with $N_t > 1$, $N_r = 1$ and maximal ratio transmission, it is $\gamma_i(t) = \sigma^2 \sum_{l=1}^{N_t} |h_{1l}^{(i)}(t)|^2$. In each of these cases, the subcarrier SNR can be written as $\gamma_i(t) = aX_D^{(i)}(t)$, where a is a constant and $X_D^{(i)}(t)$ is a Chi-squared RV with D degrees of freedom. Specifically, $a = \frac{\sigma^2}{2}$ and $D = 2$ for SISO, $a = \frac{\sigma^2}{2}$ and $D = 2N_r$ for SIMO, and $a = \frac{\sigma^2}{2}$ and $D = 2N_t$ for MISO. For single-stream multiple-input-multiple-output (MIMO), $\gamma_i(t) = \sigma^2 \zeta_i(t)$, where $\zeta_i(t)$ is the largest singular value of the channel matrix $\mathbf{H}_i(t)$, whose (k, l) th element is $h_{k,l}^{(i)}(t)$. Using the Chi-squared approximation for $\zeta_i(t)$ proposed in [26], we get $a = \frac{\sigma^2}{2} \left(\frac{N_t + N_r}{N_t N_r + 1} \right)^{\frac{2}{3}}$ and $D = 2N_t N_r$.²

We note that the Chi-squared distribution is a special case of the gamma distribution. Specifically, $\gamma_i(t) = aX_D^{(i)}(t)$ is a gamma distributed RV with shape parameter $q = \frac{D}{2}$ and scale parameter $p = 2a$. Further, the joint distribution of $\gamma_i(t)$ and $\gamma_j(t + \tau)$ is bivariate gamma since the complex channel gains at times t and $t + \tau$ are jointly Gaussian.

B. EESM-Based AMC

We focus on the practically relevant case of discrete rate adaptation, in which there are L MCSs [2], [3]. Let r_m denote the rate of MCS m and, without loss of generality, $0 < r_1 \leq r_2 \leq \dots \leq r_L$. The AMC scheme selects an MCS to maximize the throughput while ensuring that the BLER at any instant is less than a target value BLER_t [2], [4], [17]. Let $\text{BLER}_{\text{AWGN}}(\cdot, m)$ denote the BLER in an AWGN channel for MCS m . Then, MCS m can be reliably supported on an AWGN channel so long as the SNR at the time of transmission exceeds T_m , where T_m is the SNR at which $\text{BLER}_{\text{AWGN}}(T_m, m) = \text{BLER}_t$.

The EESM-based AMC proceeds as follows [4], [18]. It chooses the highest rate MCS at time t if $\gamma_{\text{eff}}^{(L)}(t) \geq T_L$. This is because the effective SNR is the equivalent flat-fading SNR and the inequality ensures that MCS L satisfies the BLER constraint. Else, the AMC scheme moves to the next highest MCS, and so on. If $\gamma_{\text{eff}}^{(i)}(t) < T_i$, for all $i = 1, \dots, L$, then no data transmission takes place because the BLER constraint cannot be satisfied. MCS 0 shall denote this scenario.

¹Note that we ignore inter-carrier interference because we are interested in channel variations over a time scale of milliseconds. This is at least one order of magnitude larger than the OFDM symbol duration.

²To focus on the impact of feedback delays on wideband rate adaptation, we do not model the outdated nature of the transmit beamforming weights [15], which are used in MISO and single-stream MIMO. Note, however, that this limitation does not apply to SIMO and open-loop MISO.

C. Throughput Analysis: Preliminaries

Let $m_{\text{opt}}(t) \in \{0, 1, \dots, L\}$ denote the MCS selected at time t . The transmission with this MCS, which occurs at time $t + \tau$, will be successful if $\gamma_{\text{eff}}^{(m_{\text{opt}}(t))}(t + \tau) \geq T_{m_{\text{opt}}(t)}$. Thus, the average throughput $\bar{R}(\tau)$ as a function of τ is given by

$$\bar{R}(\tau) = \sum_{m=1}^L r_m \Pr\{m_{\text{opt}}(t) = m, \gamma_{\text{eff}}^{(m)}(t + \tau) \geq T_m\}. \quad (2)$$

MCS m is selected if its effective SNR is greater than or equal to T_m and the effective SNRs of all the higher rate MCSs are less than their respective SNR thresholds. Thus,

$$\begin{aligned} & \Pr\{m_{\text{opt}}(t) = m, \gamma_{\text{eff}}^{(m)}(t + \tau) \geq T_m\} \\ &= P\left(\gamma_{\text{eff}}^{(m)}(t) \geq T_m, \gamma_{\text{eff}}^{(m+1)}(t) < T_{m+1}, \right. \\ & \quad \left. \dots, \gamma_{\text{eff}}^{(L)}(t) < T_L, \gamma_{\text{eff}}^{(m)}(t + \tau) \geq T_m\right). \quad (3) \end{aligned}$$

An $(L - m + 2)$ -dimensional joint distribution of the correlated RVs $\gamma_{\text{eff}}^{(m)}(t)$, $\gamma_{\text{eff}}^{(m+1)}(t)$, \dots , $\gamma_{\text{eff}}^{(L)}(t)$, and $\gamma_{\text{eff}}^{(m)}(t + \tau)$ is required to evaluate (3). However, no closed-form is known even for the marginal (one-dimensional) PDF. These RVs are correlated because they are obtained using different β_m from the same two vectors of subcarrier SNRs at times t and $t + \tau$. We circumvent this problem by using the following approximation, which is derived in Appendix A:

$$\begin{aligned} & \Pr\{m_{\text{opt}}(t) = m, \gamma_{\text{eff}}^{(m)}(t + \tau) \geq T_m\} \\ & \approx P\left(\gamma_{\text{eff}}^{(m)}(t) \geq T_m, \gamma_{\text{eff}}^{(m)}(t + \tau) \geq T_m\right) \\ & \quad - P\left(\gamma_{\text{eff}}^{(m+1)}(t) \geq T_{m+1}, \gamma_{\text{eff}}^{(m)}(t + \tau) \geq T_m\right). \quad (4) \end{aligned}$$

The accuracy of the approximation in (4) depends on how close $\gamma_{\text{eff}}^{(m)}(t)$ and $\gamma_{\text{eff}}^{(m+1)}(t)$ are, which, in turn, depends on β_m and β_{m+1} . Since the calibrated values of β_m for adjacent MCSs are close to each other [23], we can expect the approximation to be accurate. Further, this approximation is provably exact for narrowband fading.

D. Novel Bivariate Distribution for EESM Evolution in Time

We see from (4) that the joint distributions of $\gamma_{\text{eff}}^{(m)}(t)$ and $\gamma_{\text{eff}}^{(m)}(t + \tau)$, as well as $\gamma_{\text{eff}}^{(m+1)}(t)$ and $\gamma_{\text{eff}}^{(m)}(t + \tau)$ are needed. We model the time evolution of EESM with the bivariate gamma distribution [19], which was motivated in Section I-B.

1) *Key Properties of Bivariate Gamma Distribution:* Let U and V be bivariate gamma RVs. Their joint PDF in terms of four parameters $q > 0$, $s > 0$, $p > 0$, and $0 \leq r \leq sp$ is

$$\begin{aligned} f_{U,V}(u, v) &= \frac{1}{r\Gamma(q)} I_{q-1}\left(2r^{-1}\sqrt{uv(sp-r)}\right) \left[\frac{uv}{sp-r}\right]^{\frac{q-1}{2}} \\ & \quad \times \exp\left(-\frac{pu+sv}{r}\right), u > 0, v > 0, \quad (5) \end{aligned}$$

where $\Gamma(\cdot)$ is the gamma function and $I_{q-1}(\cdot)$ is the $(q-1)$ th-order modified Bessel function of first kind [25]. The joint CDF is given by

$$\begin{aligned} F_{U,V}(u, v) &= \frac{r^q}{\Gamma(q)} \sum_{k=0}^{\infty} \frac{(sp-r)^k \Gamma(k+q)}{k!(sp)^{k+q}} \Gamma_{\text{inc}}\left(k+q, u\frac{p}{r}\right) \\ & \quad \times \Gamma_{\text{inc}}\left(k+q, v\frac{s}{r}\right), u > 0, v > 0, \quad (6) \end{aligned}$$

where $\Gamma_{\text{inc}}(q, a) = \frac{1}{\Gamma(q)} \int_0^a x^{q-1} \exp(-x) dx$ is the incomplete gamma function [25]. The RVs U and V are gamma distributed with parameters q and s , and q and p , respectively. Their PDF is given in [19]. The conditional CDF $F_V(v|u)$ is

$$\begin{aligned} F_V(v|u) &= \exp\left(-u\frac{sp-r}{sr}\right) \sum_{k=0}^{\infty} \frac{u^k}{k!} \left(\frac{sp-r}{sr}\right)^k \\ & \quad \times \Gamma_{\text{inc}}\left(k+q, \frac{sv}{r}\right), u > 0, v > 0. \quad (7) \end{aligned}$$

Lastly, the joint MGF $\Psi_{U,V}(\cdot, \cdot)$ of U and V is given by

$$\begin{aligned} \Psi_{U,V}(z_1, z_2) &= (1 + sz_1 + pz_2 + rz_1z_2)^{-q}, \\ & \quad \text{for } sz_1 + pz_2 + rz_1z_2 > -1. \quad (8) \end{aligned}$$

2) *Computing the Bivariate Gamma Parameters:* Since we are interested in the joint PDF of $\gamma_{\text{eff}}^{(m_1)}(t)$ and $\gamma_{\text{eff}}^{(m_2)}(t + \tau)$, we introduce subscripts m_1 and m_2 into the notations for the four distribution parameters, and henceforth denote them as q_{m_1, m_2} , s_{m_1, m_2} , p_{m_1, m_2} , and r_{m_1, m_2} . To express them in terms of a , D , N_{sc} , and \mathbf{C} , we propose matching the joint MGF of $\gamma_{\text{eff}}^{(m_1)}(t)$ and $\gamma_{\text{eff}}^{(m_2)}(t + \tau)$ with that of the bivariate gamma distribution at four carefully chosen points as follows.

Let $Y_m(t) = \frac{1}{N_{\text{sc}}} \sum_{i=1}^{N_{\text{sc}}} \exp\left(-\frac{\gamma_i(t)}{\beta_m}\right)$. Then, $\Psi_{\gamma_{\text{eff}}^{(m)}(t)}(z) = \mathbb{E}[(Y_m(t))^{z\beta_m}]$. Using (8), we get the following relationships:

$$\begin{aligned} \mathbb{E}[Y_{m_1}(t)] &= \Psi_{\gamma_{\text{eff}}^{(m_1)}(t), \gamma_{\text{eff}}^{(m_2)}(t+\tau)}(\beta_{m_1}^{-1}, 0) \\ &= (1 + s_{m_1, m_2} \beta_{m_1}^{-1})^{-q_{m_1, m_2}}, \quad (9) \end{aligned}$$

$$\begin{aligned} \mathbb{E}[Y_{m_1}^2(t)] &= \Psi_{\gamma_{\text{eff}}^{(m_1)}(t), \gamma_{\text{eff}}^{(m_2)}(t+\tau)}(2\beta_{m_1}^{-1}, 0) \\ &= (1 + 2s_{m_1, m_2} \beta_{m_1}^{-1})^{-q_{m_1, m_2}}, \quad (10) \end{aligned}$$

$$\begin{aligned} \mathbb{E}[Y_{m_2}(t)] &= \Psi_{\gamma_{\text{eff}}^{(m_1)}(t), \gamma_{\text{eff}}^{(m_2)}(t+\tau)}(0, \beta_{m_2}^{-1}) \\ &= (1 + p_{m_1, m_2} \beta_{m_2}^{-1})^{-q_{m_1, m_2}}, \quad (11) \end{aligned}$$

$$\begin{aligned} & \mathbb{E}[Y_{m_1}(t)Y_{m_2}(t + \tau)] \\ &= \Psi_{\gamma_{\text{eff}}^{(m_1)}(t), \gamma_{\text{eff}}^{(m_2)}(t+\tau)}(\beta_{m_1}^{-1}, \beta_{m_2}^{-1}) \\ &= \left[1 + \frac{s_{m_1, m_2}}{\beta_{m_1}} + \frac{p_{m_1, m_2}}{\beta_{m_2}} + \frac{r_{m_1, m_2}}{\beta_{m_1}\beta_{m_2}}\right]^{-q_{m_1, m_2}}. \quad (12) \end{aligned}$$

From (9) and (10), we obtain the following non-linear equation involving s_{m_1, m_2} : $1 + 2\beta_{m_1}^{-1}s_{m_1, m_2} = (1 + \beta_{m_1}^{-1}s_{m_1, m_2})^\delta$, where $\delta = \log(\mathbb{E}[Y_{m_1}^2(t)]) / \log(\mathbb{E}[Y_{m_1}(t)]) > 1$. There exists a unique non-zero value of s_{m_1, m_2} that solves it and is computed

numerically. Given s_{m_1, m_2} , the remaining parameters can be written in closed-form as follows:³

$$q_{m_1, m_2} = -\frac{\log(\mathbb{E}[Y_{m_1}(t)])}{\log(1 + \beta_{m_1}^{-1} s_{m_1, m_2})}, \quad (13)$$

$$p_{m_1, m_2} = \beta_{m_2} (\mathbb{E}[Y_{m_2}(t)])^{-\frac{1}{q_{m_1, m_2}}} - \beta_{m_2}, \quad (14)$$

$$r_{m_1, m_2} = \beta_{m_1} \beta_{m_2} (\mathbb{E}[Y_{m_1}(t)Y_{m_2}(t + \tau)])^{-\frac{1}{q_{m_1, m_2}}} - \beta_{m_1} p_{m_1, m_2} - \beta_{m_2} s_{m_1, m_2} - \beta_{m_1} \beta_{m_2}. \quad (15)$$

3) *Moments of $Y_{m_1}(t)$ and $Y_{m_2}(t + \tau)$* : Thus, all that remains to be done is to compute the moments $\mathbb{E}[Y_{m_1}(t)]$, $\mathbb{E}[Y_{m_2}(t)]$, $\mathbb{E}[Y_{m_1}^2(t)]$, and $\mathbb{E}[Y_{m_1}(t)Y_{m_2}(t + \tau)]$. These are given in closed-form below.

Result 1: The first two moments of $Y_m(t)$ for $m = m_1, m_2$, when $\gamma_i(t) = aX_D^{(i)}(t)$, are given by

$$\mathbb{E}[Y_m(t)] = (1 + 2a\beta_m^{-1})^{-\frac{D}{2}}, \quad (16)$$

$$\mathbb{E}[Y_m^2(t)] = \frac{1}{N_{sc}^2} \sum_{i=1}^{N_{sc}} \sum_{j=1}^{N_{sc}} \times \left[(1 + 2a\beta_m^{-1})^2 - 4a^2 |C_{ij}|^2 \beta_m^{-2} \right]^{-\frac{D}{2}}. \quad (17)$$

The cross-correlation between $Y_{m_1}(t)$ and $Y_{m_2}(t + \tau)$ equals

$$\begin{aligned} \mathbb{E}[Y_{m_1}(t)Y_{m_2}(t + \tau)] &= \frac{1}{N_{sc}^2} \sum_{i=1}^{N_{sc}} \sum_{j=1}^{N_{sc}} \left[(1 + 2a\beta_{m_1}^{-1}) (1 + 2a\beta_{m_2}^{-1}) \right. \\ &\quad \left. - 4\rho(\tau)a^2 |C_{ij}|^2 \beta_{m_1}^{-1} \beta_{m_2}^{-1} \right]^{-\frac{D}{2}}. \quad (18) \end{aligned}$$

Proof: The proof is relegated to Appendix B. ■

E. Empirical Verification of the Proposed Bivariate Model

For empirical verification, we consider independent subcarriers and correlated subcarriers like those in the standardized typical urban (TU) and the rural area (RA) channels [27]. First, we compare the empirical CDF curves with those obtained from the proposed model, as has been done in the literature [21], [24]. In our problem, the joint CDF plots are three-dimensional. We, therefore, plot the conditional CDF of $\gamma_{\text{eff}}^{(m_2)}(t + \tau)$ given $\gamma_{\text{eff}}^{(m_1)}(t)$ for different values of $\gamma_{\text{eff}}^{(m_1)}(t)$, and compare it with the empirical conditional CDF.

Figs. 2 and 3 compare the conditional CDFs for independent subcarriers and correlated subcarriers from the TU channel, respectively. The bivariate lognormal parameters are obtained by matching the joint MGF of $\gamma_{\text{eff}}^{(m_1)}(t)$ and $\gamma_{\text{eff}}^{(m_2)}(t + \tau)$ with that of the bivariate lognormal. As mentioned, corresponding results for the beta [18], GEV, and Pearson [20] models cannot be shown because no tractable bivariate extension is known for

³We observe from (9), (10), (11), and (12) that the ordering of the RVs matters in determining the parameters. In case $r_{m_1, m_2} < 0$, we compute the parameters of the ordered pair $(\gamma_{\text{eff}}^{(m_2)}(t + \tau), \gamma_{\text{eff}}^{(m_1)}(t))$ instead.

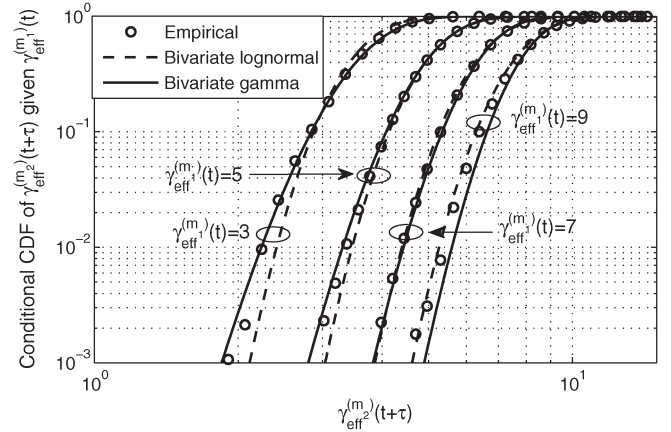


Fig. 2. Comparison of the conditional CDFs of EESM with the proposed bivariate gamma distribution for independent subcarriers ($\sigma^2 = 10$ dB, $N_{sc} = 12$, $\beta_{m_1} = \beta_{m_2} = 5$, $D = 2$, and $f_d\tau = 0.1$).

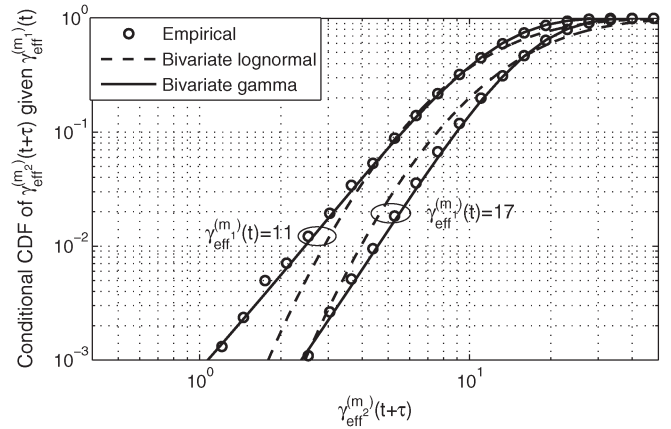


Fig. 3. Comparison of the conditional CDFs of EESM with the proposed bivariate gamma distribution for the TU channel ($\sigma^2 = 10$ dB, $N_{sc} = 12$, $\beta_{m_1} = \beta_{m_2} = 5$, $D = 4$, and $f_d\tau = 0.1$).

them. Notice that the bivariate gamma model tracks the empirical curves well over a wide range of values from 10^{-3} to 1. While the proposed model is more accurate than the bivariate lognormal model for smaller values of $\gamma_{\text{eff}}^{(m_1)}(t)$, the reverse is true for larger values of $\gamma_{\text{eff}}^{(m_1)}(t)$. For the TU channel, however, the bivariate gamma model is much more accurate than the bivariate lognormal model in all regimes. The accuracy is even better for the less dispersive RA channel; results for which are not shown due to space constraints.

An alternate way to evaluate the efficacy is to compare the Kulback-Leibler (KL) divergence of the joint PDF obtained from the model and the empirical joint PDF [28] as shown in Table I. The smaller the KL divergence, the better the approximation. This is because the KL divergence is always non-negative, and is zero if and only if the two distributions are identical. Further, the KL divergence between continuous distributions evaluated from their empirical distributions converges almost surely [29]. However, we note that it is not a true distance metric because it is not symmetrical and it does not satisfy the triangle inequality [28]. We see that the KL divergences of the two distributions are close to each other for independent subcarriers, indicating a comparable performance.

TABLE I
KL DIVERGENCES FOR BIVARIATE GAMMA AND BIVARIATE
LOGNORMAL DISTRIBUTIONS ($\sigma^2 = 10$, $N_{sc} = 12$, AND $D = 4$)

	Independent subcarriers	TU channel	RA channel
Bivariate gamma vs. empirical	0.0455	0.0587	0.0622
Bivariate lognormal vs. empirical	0.0228	0.2720	0.3529

However, for the TU and RA channels, the KL divergence of the proposed model is lower by a factor of 4.60 and 5.78, respectively, indicating a better approximation.

F. Average Throughput Analysis

Using the bivariate model for EESM developed above, we now derive an expression for the average throughput.

Result 2: The average throughput as a function of feedback delay is given by (21), shown at the bottom of the page, where $\xi_{m_1, m_2} = \frac{r_{m_1, m_2}}{s_{m_1, m_2} p_{m_1, m_2}}$, for $m_1, m_2 \in \{m, m+1\}$ and $T_{L+1} = \infty$.

We note that the above expression is exact in a narrowband fading channel since all the subcarrier gains are equal, and can be obtained by setting $N_{sc} = 1$. In the absence of feedback delays ($\tau = 0$), the average throughput is given by

$$\bar{R}(0) \approx \sum_{m=1}^L r_m \left[\Gamma_{\text{inc}}(q_{m+1, m}, T_{m+1} s_{m+1, m}^{-1}) - \Gamma_{\text{inc}}(q_{m, m}, T_m s_{m, m}^{-1}) \right]. \quad (19)$$

III. MULTI-CELL, MULTI-USER SCENARIO WITH FREQUENCY-DOMAIN SCHEDULING

We now focus on downlink transmission in a multi-cell, multi-user system with co-channel interference and in which all links undergo both shadowing and fading. There are K users per cell. Full frequency reuse is assumed [2]. Multiple users now vie for each resource block (RB), which consists of N_{sc} subcarriers. Users estimate the channel gains on the N_{sc} subcarriers, and uses the EESM-based AMC scheme to select the MCS to be fed back to the BS. The frequency-domain scheduler at the BS assigns users to RBs. The scheduled user is served with the rate reported by it. Thus, *the reported MCSs are used for both scheduling and rate adaptation*. The notation in this section will be more elaborate as it needs to track the user as well as the BS index. Let $h_{uv}^{(n, k, j)}(t)$ denote the channel gain

from transmit antenna v of BS j to receive antenna u of user k of subcarrier n at time t .

We first develop the theory for a SISO system ($u = 1$ and $v = 1$), and then extend it to include multi-antenna diversity. Thus, the SINR $\gamma_k^{(n)}(t)$ on the n th subcarrier, $1 \leq n \leq N_{sc}$, for the scheduled user, say k , at time t is given by

$$\gamma_k^{(n)}(t) = \frac{P_S}{P_N} \frac{\alpha_{0k} |h_{11}^{(n, k, 0)}(t)|^2}{\sum_{j=1}^M \frac{P_S}{P_N} \alpha_{jk} |h_{11}^{(n, k, j)}(t)|^2 + 1}, \quad (20)$$

where P_S is the BS transmit power, P_N is the noise power, and M is the number of interfering BSs. Here, $\sqrt{\alpha_{0k}} h_{11}^{(n, k, 0)}(t)$ and $\sqrt{\alpha_{jk}} h_{11}^{(n, k, j)}(t)$ denote the complex channel gains at time t from the serving BS 0 and interfering BS j , respectively. They are assumed to be independent as the BSs are located far apart [3], [24]. The model for the small-scale fading term $h_{11}^{(n, k, j)}(t)$ is the same as in Section II-A. The lognormal RV α_{jk} models shadowing. Thus, in dB scale, α_{jk} is a Gaussian RV with mean $\mu_{jk} = -L_0 - 10\eta \log(d_{jk}/d_0)$ and standard deviation σ_{shad} , where L_0 is the pathloss in dB at a reference distance d_0 from the BS, d_{jk} is the distance between user k and BS j , and η is the pathloss exponent.⁴ Notice that different users see statistically different interferences. Let $\gamma_{\text{eff}}^{(k, m)}(t)$ denote the effective SNR for MCS m and user k at time t and $\beta_{k, m}$ denote the corresponding MCS-dependent parameter.

A. New Bivariate Gamma Mixture Model for EESM Time Evolution

As in the point-to-point scenario, we first develop a tractable and accurate bivariate model for the time variation of EESM. With shadowing and co-channel interference, the subcarrier SINR $\gamma_k^{(n)}(t)$ in (20) is no longer gamma distributed. Consequently, the bivariate gamma model proposed in Section II-D is no longer suitable and a more general model is required.

Consider the interference plus noise term in (20), which we denote by $\Omega_k^{(n)}(t) = \sum_{j=1}^M (P_S/P_N) \alpha_{jk} |h_{11}^{(n, k, j)}(t)|^2 + 1$. Using the result that the sum of Rayleigh-lognormal RVs is well approximated by a lognormal [21], we approximate $\Omega_k^{(n)}(t)$ with a lognormal RV. Further, for tractability, we ignore its variation with time and frequency. This is partially justified because

⁴Time variation in shadowing is ignored because it is several orders of magnitude slower than in small-scale fading.

$$\begin{aligned} \bar{R}(\tau) \approx \sum_{m=1}^L r_m \left\{ \sum_{k=0}^{\infty} \left[\frac{(\xi_{m, m})^{q_{m, m}} (1 - \xi_{m, m})^k \Gamma(k + q_{m, m})}{k! \Gamma(q_{m, m})} \Gamma_{\text{inc}} \left(k + q_{m, m}, \frac{T_m p_{m, m}}{r_{m, m}} \right) \Gamma_{\text{inc}} \left(k + q_{m, m}, \frac{T_m s_{m, m}}{r_{m, m}} \right) \right. \right. \\ \left. \left. - \frac{(\xi_{m+1, m})^{q_{m+1, m}} (1 - \xi_{m+1, m})^k \Gamma(k + q_{m+1, m})}{k! \Gamma(q_{m+1, m})} \Gamma_{\text{inc}} \left(k + q_{m+1, m}, \frac{T_{m+1} p_{m+1, m}}{r_{m+1, m}} \right) \right. \right. \\ \left. \left. \times \Gamma_{\text{inc}} \left(k + q_{m+1, m}, \frac{T_m s_{m+1, m}}{r_{m+1, m}} \right) \right] + \Gamma_{\text{inc}} \left(q_{m+1, m}, \frac{T_{m+1}}{s_{m+1, m}} \right) - \Gamma_{\text{inc}} \left(q_{m, m}, \frac{T_m}{s_{m, m}} \right) \right\} \quad (21) \end{aligned}$$

$\Omega_k^{(n)}(t)$ is a sum of M independent RVs, which averages out the time-frequency variations due to small-scale fading. Thus, $\Omega_k^{(n)}(t) \approx \alpha_{\Omega_k}$, where α_{Ω_k} is a lognormal RV, whose dB mean μ_{Ω_k} and dB variance $\sigma_{\Omega_k}^2$ are obtained by matching the MGF of $\Omega_k^{(n)}(t)$ with that of the lognormal distribution. We shall verify its accuracy in Section IV-B. The MGF of $\Omega_k^{(n)}(t)$ is derived in Appendix C and is given by

$$\Psi_{\Omega_k^{(n)}(t)}(z) \approx \frac{e^{-z}}{\pi^{\frac{M}{2}}} \prod_{j=1}^M \left[\sum_{i=1}^{N_{GH}} \frac{w_i}{1 + z \frac{P_S}{P_N} e^{\mu_{j,k}} + \sqrt{2} \sigma_{\text{shad}} \lambda_i} \right], \quad (22)$$

for $z \geq 0$. Here, w_i , λ_i , and N_{GH} are the weights, abscissas, and Gauss-Hermite integration order, respectively [30].

Therefore, the SINR of subcarrier n in (20) can be written as $\gamma_k^{(n)}(t) = (P_S/P_N)\varphi_k X_2^{(n,k)}(t)$, where φ_k is a lognormal RV with dB mean $\mu_{\varphi_k} = \mu_{0k} - \mu_{\Omega_k}$ and dB variance $\sigma_{\varphi_k}^2 = \sigma_{\text{shad}}^2 + \sigma_{\Omega_k}^2$, and $X_2^{(n,k)}(t) = |h_{11}^{(n,k,0)}(t)|^2$ is a Chi-squared RV with two degrees of freedom. For the simpler single-cell scenario [18], [24], in which there is no co-channel interference, the dB mean and dB variance of φ_k simplify to μ_{0k} and σ_{shad}^2 , respectively.

The bivariate PDF of the RVs $\gamma_{\text{eff}}^{(k,m_1)}(t)$ and $\gamma_{\text{eff}}^{(k,m_2)}(t+\tau)$ can be obtained by averaging its PDF conditioned on φ_k , i.e., $f_{\gamma_{\text{eff}}^{(k,m_1)}(t), \gamma_{\text{eff}}^{(k,m_2)}(t+\tau)}(x, y | \varphi_k = \alpha)$. It is given by

$$\begin{aligned} & f_{\gamma_{\text{eff}}^{(k,m_1)}(t), \gamma_{\text{eff}}^{(k,m_2)}(t+\tau)}(x, y) \\ &= \int_0^\infty f_{\gamma_{\text{eff}}^{(k,m_1)}(t), \gamma_{\text{eff}}^{(k,m_2)}(t+\tau)}(x, y | \varphi_k = \alpha) \\ & \quad \times \frac{1}{\sqrt{2\pi}\sigma_{\varphi_k}\alpha} e^{-\frac{(\log(\alpha) - \mu_{\varphi_k})^2}{2\sigma_{\varphi_k}^2}} d\alpha. \end{aligned} \quad (23)$$

Using Gauss-Hermite quadrature [30] followed by scaling the resulting expression so that the PDF integrates to 1, we get

$$\begin{aligned} & f_{\gamma_{\text{eff}}^{(k,m_1)}(t), \gamma_{\text{eff}}^{(k,m_2)}(t+\tau)}(x, y) \\ &= \sum_{i=1}^{N_{GH}} \tilde{w}_i f_{\gamma_{\text{eff}}^{(k,m_1)}(t), \gamma_{\text{eff}}^{(k,m_2)}(t+\tau)}(x, y | \varphi_k = \varpi^{(k,i)}), \end{aligned} \quad (24)$$

where $\tilde{w}_i = w_i / \sum_{j=1}^{N_{GH}} w_j$ and $\varpi^{(k,i)} = e^{\mu_{\varphi_k} + \sqrt{2}\sigma_{\varphi_k}\lambda_i}$.

Note that, given $\varphi_k = \varpi^{(k,i)}$, for $1 \leq i \leq N_{GH}$ and $1 \leq k \leq K$, the subcarrier SINR is a scaled Chi-squared RV of the form $\gamma_k^{(n,i)}(t) = (P_S/P_N)\varpi^{(k,i)} X_2^{(n,k)}(t)$, for $1 \leq n \leq N_{\text{sc}}$. Thus, from Section II-D, the conditional PDF $f_{\gamma_{\text{eff}}^{(k,m_1)}(t), \gamma_{\text{eff}}^{(k,m_2)}(t+\tau)}(x, y | \varphi_k = \varpi^{(k,i)})$ can be accurately approximated by the bivariate gamma distribution. Let $q_{m_1, m_2}^{(k,i)}$, $s_{m_1, m_2}^{(k,i)}$, $p_{m_1, m_2}^{(k,i)}$, and $r_{m_1, m_2}^{(k,i)}$ denote its distribution parameters. Note that the notation for these parameters has been updated to track the user (k) and the Gauss-quadrature term (i). These are obtained by matching the joint MGF of $\gamma_{\text{eff}}^{(k,m_1)}(t)$ and $\gamma_{\text{eff}}^{(k,m_2)}(t+\tau)$ conditioned on $\varphi_k = \varpi^{(k,i)}$ at four points with

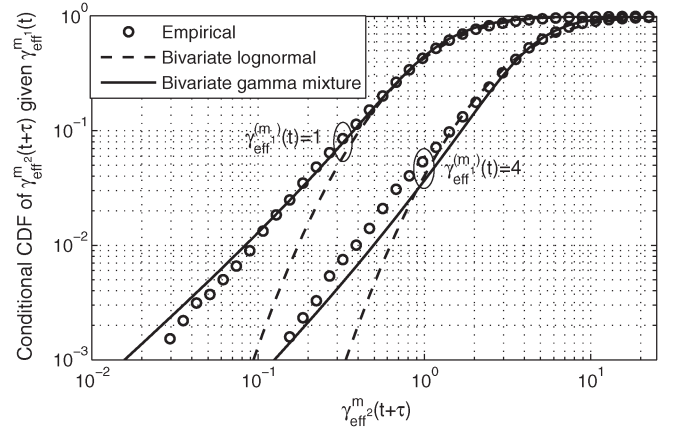


Fig. 4. Comparison of the conditional CDFs of EESM with the proposed bivariate gamma mixture distribution in the TU channel ($N_{\text{sc}} = 12$, $\beta_{m_1} = \beta_{m_2} = 5$, and $f_d\tau = 0.1$).

the joint MGF of the bivariate gamma distribution, as in (9), (10), (11), and (12).

Putting all the above steps together, we get

$$\begin{aligned} & f_{\gamma_{\text{eff}}^{(k,m_1)}(t), \gamma_{\text{eff}}^{(k,m_2)}(t+\tau)}(x, y) \\ &= \sum_{i=1}^{N_{GH}} \frac{\tilde{w}_i}{r_{m_1, m_2}^{(k,i)} \Gamma(q_{m_1, m_2}^{(k,i)})} \exp\left(-\frac{xp_{m_1, m_2}^{(k,i)} + ys_{m_1, m_2}^{(k,i)}}{r_{m_1, m_2}^{(k,i)}}\right) \\ & \quad \times I_{q_{m_1, m_2}^{(k,i)} - 1} \left(2\sqrt{\frac{xy \left(s_{m_1, m_2}^{(k,i)} p_{m_1, m_2}^{(k,i)} - r_{m_1, m_2}^{(k,i)} \right)}{r_{m_1, m_2}^{(k,i)}}} \right) \\ & \quad \times \left[\frac{xy}{s_{m_1, m_2}^{(k,i)} p_{m_1, m_2}^{(k,i)} - r_{m_1, m_2}^{(k,i)}} \right]^{\frac{q_{m_1, m_2}^{(k,i)} - 1}{2}}, \quad x, y > 0. \end{aligned} \quad (25)$$

Notice that (25) is a weighted sum of bivariate gamma distributions. This approach generalizes the bivariate gamma model of the previous section. It can be extended to SIMO and MISO by replacing $X_2^{(n,k)}(t)$ with a Chi-squared RV with D degrees of freedom $X_D^{(n,k)}(t)$. For single-stream MIMO, $X_2^{(n,k)}(t)$ is replaced with $\left(\frac{N_t + N_r}{N_t N_r + 1}\right)^{\frac{2}{3}} X_D^{(n,k)}(t)$ (cf. Section II-A). While the gamma mixture distribution has been used in [31], the novelty in our work lies in developing the mixture approach for modeling—for the first time—the time-evolution of EESM and showing that it works well.

B. Empirical Verification of the Bivariate Mixture Model

As in Section II-D, we plot the conditional CDFs to evaluate the accuracy of the proposed model. We use $\frac{P_S}{P_N} = 10$, $\mu_{\varphi_k} = 0$, $\sigma_{\varphi_k} = 8$ dB, and the TU channel. Fig. 4 plots the empirical conditional CDFs and those from the proposed mixture distribution. The conditional CDFs of the bivariate lognormal distribution are also plotted for benchmarking. We see that the proposed model, while not perfect, does track the empirical conditional CDFs well, and is better than the bivariate lognormal distribution.

C. Cell Throughput Analysis With Different Schedulers

We now analyze cell throughput per RB, which is the sum-throughput of all the users in the reference cell 0 with feedback delays. This is done for the following three different frequency-domain schedulers, which cover a wide range of the trade-off between throughput and fairness:

- 1) *RR scheduler* [13]: It schedules the users in a periodic manner for each RB. Thus, channel quality feedback is used for rate adaptation, but not for scheduling.
- 2) *Greedy scheduler* [10]: For each RB, it assigns the user that reported the highest rate among all the users to it. In case multiple users report the highest rate, then one among them is chosen with equal probability. While this scheduler maximizes throughput, it is unfair as users closer to the BS get scheduled more often.
- 3) *MPF scheduler*: It selects the user with the highest ratio of rate reported to its fading-averaged value [22]. It has a throughput-fairness trade-off similar to the PF scheduler proposed in [32], and is often studied as it is tractable [9], [18], [22].

Let $R_k(t)$ denote the rate reported by user k and S_t denote the scheduled user, at time t . The cell throughput $C(\tau)$ is

$$C(\tau) = \sum_{k=1}^K \sum_{m=1}^L r_m P\left(R_k(t) = r_m, \gamma_{\text{eff}}^{(k,m)}(t+\tau) \geq T_m\right) \times P\left(S_t = k | R_k(t) = r_m, \gamma_{\text{eff}}^{(k,m)}(t+\tau) \geq T_m\right). \quad (26)$$

Note that S_t depends only on $R_1(t), \dots, R_K(t)$, which are independent RVs. Thus, conditioned on the rate reported at time t by a user, its effective SINR at time $t+\tau$ is independent of the scheduling decision. Thus, (26) simplifies to

$$C(\tau) = \sum_{k=1}^K \sum_{m=1}^L r_m P\left(R_k(t) = r_m, \gamma_{\text{eff}}^{(k,m)}(t+\tau) \geq T_m\right) \times P\left(S_t = k | R_k(t) = r_m\right). \quad (27)$$

Here, $P(R_k(t) = r_m, \gamma_{\text{eff}}^{(k,m)}(t+\tau) \geq T_m)$ is the probability of a successful transmission by user k with MCS m for a

feedback delay of τ . Its expression in terms of the bivariate CDFs of $\gamma_{\text{eff}}^{(m)}(t)$ and $\gamma_{\text{eff}}^{(m)}(t+\tau)$, and $\gamma_{\text{eff}}^{(m+1)}(t)$ and $\gamma_{\text{eff}}^{(m)}(t+\tau)$ is given in (4). Using (25) the expression for $P(R_k(t) = r_m, \gamma_{\text{eff}}^{(k,m)}(t+\tau) \geq T_m)$ is given by (30), shown at the bottom of page, where $\xi_{m_1, m_2}^{(k,i)} = r_{m_1, m_2}^{(k,i)} (s_{m_1, m_2}^{(k,i)} p_{m_1, m_2}^{(k,i)})^{-1}$.

We now evaluate $P(S_t = k | R_k(t) = r_m)$ for each scheduler, which together with (30) yields the expression for $C(\tau)$.

Result 3: The expression for the conditional probability $P(S_t = k | R_k(t) = r_m)$ is as follows:

RR scheduler: $P(S_t = k | R_k(t) = r_m) = 1/K$.

Greedy scheduler: It is given by

$$P(S_t = k | R_k(t) = r_m) = \sum_{v=1}^{K-1} \frac{1}{v+1} \sum_{\substack{n_1=1 \\ n_1 \neq k}}^K \cdots \sum_{\substack{n_v=n_{v-1}+1 \\ n_v \neq k}}^K \prod_{g \in \{n_1, \dots, n_v\}} \left[\sum_{i=1}^{N_{GH}} \tilde{w}_i \left\{ \Gamma_{\text{inc}}\left(q_{m+1, m}^{(g,i)}, \frac{T_{m+1}}{s_{m+1, m}^{(g,i)}}\right) - \Gamma_{\text{inc}}\left(q_{m, m}^{(g,i)}, \frac{T_m}{s_{m, m}^{(g,i)}}\right) \right\} \right] \times \prod_{\substack{h=1 \\ h \notin \{k, n_1, \dots, n_v\}}}^K \left[\sum_{i=1}^{N_{GH}} \tilde{w}_i \Gamma_{\text{inc}}\left(q_{m, m}^{(h,i)}, \frac{T_m}{s_{m, m}^{(h,i)}}\right) \right] + \prod_{\substack{g=1 \\ g \neq k}}^K \left[\sum_{i=1}^{N_{GH}} \tilde{w}_i \Gamma_{\text{inc}}\left(q_{m, m}^{(g,i)}, \frac{T_m}{s_{m, m}^{(g,i)}}\right) \right]. \quad (28)$$

MPF scheduler: Let m_{gk} denote the index of the highest rate that is strictly less than $r_m \mathbb{E}[R_g(t)] / \mathbb{E}[R_k(t)]$. Then,

$$P(S_t = k | R_k(t) = r_m) = \prod_{\substack{g=1 \\ g \neq k}}^K \left[\sum_{i=1}^{N_{GH}} \tilde{w}_i \Gamma_{\text{inc}}\left(q_{m_{gk}+1, m_{gk}+1}^{(g,i)}, \frac{T_{m_{gk}+1}}{s_{m_{gk}+1, m_{gk}+1}^{(g,i)}}\right) \right]. \quad (29)$$

Proof: The proof is relegated to Appendix D.

$$P\left(R_k(t) = r_m, \gamma_{\text{eff}}^{(k,m)}(t+\tau) \geq T_m\right) \approx \sum_{i=1}^{N_{GH}} \tilde{w}_i \sum_{j=0}^{\infty} \left\{ \frac{\left(1 - \xi_{m, m}^{(k,i)}\right)^j \left(\xi_{m, m}^{(k,i)}\right)^{q_{m, m}^{(k,i)}} \Gamma\left(j + q_{m, m}^{(k,i)}\right)}{j! \Gamma\left(q_{m, m}^{(k,i)}\right)} \Gamma_{\text{inc}}\left(j + q_{m, m}^{(k,i)}, \frac{T_m p_{m, m}^{(k,i)}}{r_{m, m}^{(k,i)}}\right) \Gamma_{\text{inc}}\left(j + q_{m, m}^{(k,i)}, \frac{T_m s_{m, m}^{(k,i)}}{r_{m, m}^{(k,i)}}\right) - \frac{\left(1 - \xi_{m+1, m}^{(k,i)}\right)^j \left(\xi_{m+1, m}^{(k,i)}\right)^{q_{m+1, m}^{(k,i)}} \Gamma\left(j + q_{m+1, m}^{(k,i)}\right)}{j! \Gamma\left(q_{m+1, m}^{(k,i)}\right)} \Gamma_{\text{inc}}\left(j + q_{m+1, m}^{(k,i)}, \frac{T_{m+1} p_{m+1, m}^{(k,i)}}{r_{m+1, m}^{(k,i)}}\right) \Gamma_{\text{inc}}\left(j + q_{m+1, m}^{(k,i)}, \frac{T_{m+1} s_{m+1, m}^{(k,i)}}{r_{m+1, m}^{(k,i)}}\right) \right\} + \sum_{i=1}^{N_{GH}} \tilde{w}_i \left[\Gamma_{\text{inc}}\left(q_{m+1, m}^{(k,i)}, \frac{T_{m+1}}{s_{m+1, m}^{(k,i)}}\right) - \Gamma_{\text{inc}}\left(q_{m, m}^{(k,i)}, \frac{T_m}{s_{m, m}^{(k,i)}}\right) \right] \quad (30)$$

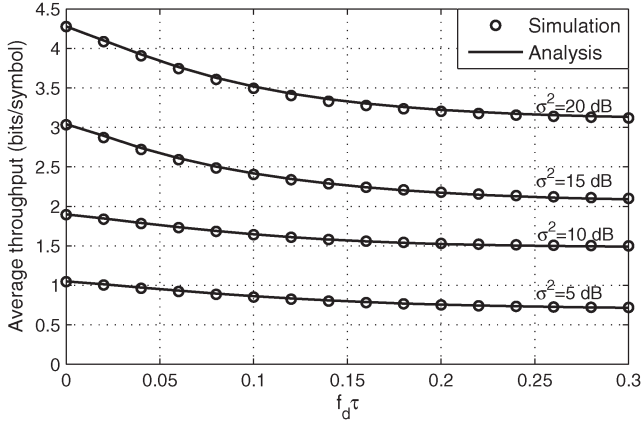


Fig. 5. Independent subcarriers: Average throughput as a function of normalized delay for different average SNRs ($N_{sc} = 24$ and $D = 2$ (SISO)).

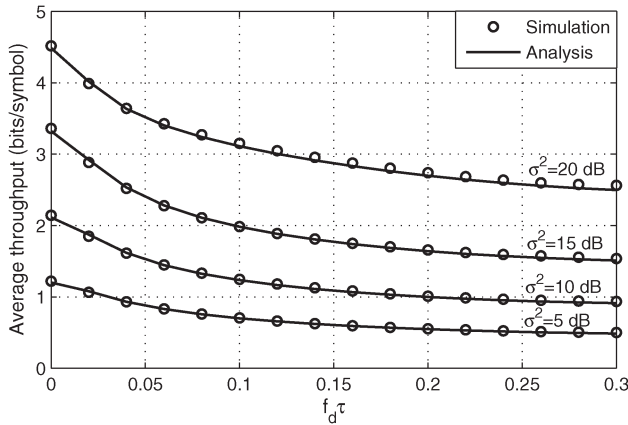


Fig. 6. RA channel: Average throughput as a function of normalized delay for different per-link average SNRs ($N_{sc} = 24$ and $D = 2$ (SISO)).

IV. NUMERICAL RESULTS

We present Monte Carlo simulation results that average over 4×10^4 samples to evaluate the accuracy of the throughput analysis and investigate the effects of different system parameters. We use $N_{sc} = 24$ subcarriers and $\text{BLER}_t = 0.1$ [2], [4]. The MCSs specified in the LTE standard are used for AMC. They are given in [23, Tbl. I] along with the β_m values and SNR thresholds. We have found that $N_{GH} = 8$ is sufficient to get results that are accurate up to three orders of magnitude. The number of terms used to evaluate the infinite series in (21) and (30) depends on $f_d\tau$ and the correlation between subcarriers.⁵ We first show results for the point-to-point scenario and then for the multi-cell, multi-user scenario.

A. Point-to-Point Scenario

The average throughput as a function of $f_d\tau$ for different Tx-Rx link average SNRs σ^2 and $D = 2$ (SISO) is shown in Fig. 5 for independent subcarriers and in Fig. 6 for the

⁵For example, for $f_d\tau = 0.1$, 20 and 100 terms are sufficient for correlated and independent subcarriers, respectively. The number of terms increases as $f_d\tau$ decreases because the subcarrier SNR is more correlated over time.

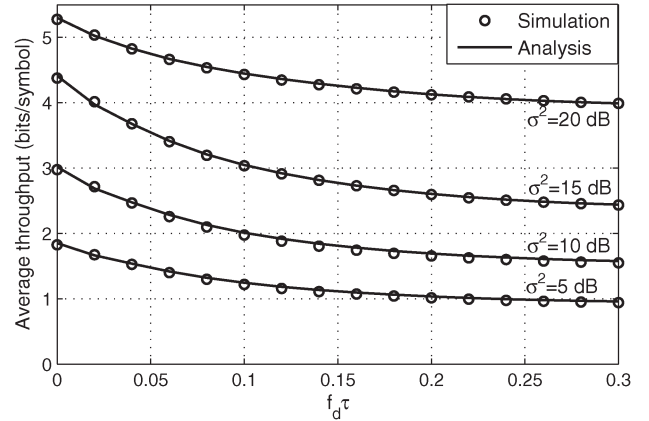


Fig. 7. TU channel: Average throughput as a function of normalized delay for different per-link average SNRs ($N_{sc} = 24$ and $D = 4$ (1×2 SIMO)).

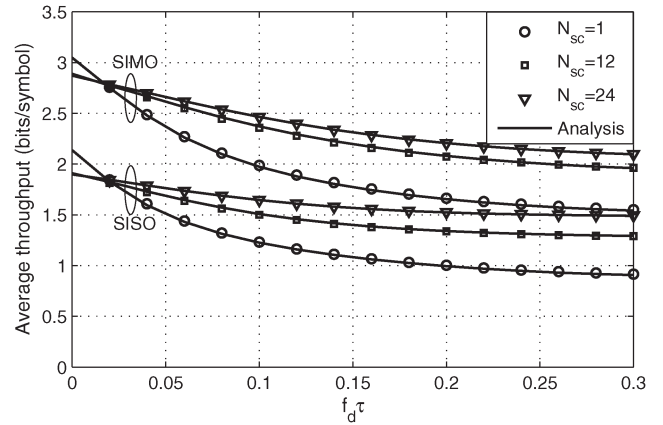


Fig. 8. Effect of number of subcarriers on average throughput as a function of normalized delay ($\sigma^2 = 10$ dB).

RA channel. Notice the good match between the analysis and the simulation results in both figures. As $f_d\tau$ increases, the average throughput decreases. For independent subcarriers, the percentage drops are 32%, 22%, and 27% for $\sigma^2 = 5$ dB, 10 dB, and 20 dB, respectively, when $f_d\tau$ increases from 0 to 0.3. The corresponding numbers for the RA channel are 59%, 57%, and 54%. Thus, the drop in the throughput with feedback delay is greater when the subcarriers are more correlated.

The average throughput versus $f_d\tau$ for the TU channel and $D = 4$ (1×2 SIMO or 2×1 MISO) is shown in Fig. 7. We again see a good match between analysis and simulations. Here, the percentage reductions in throughput are 48%, 48%, and 25%, respectively, for $\sigma^2 = 5$ dB, 10 dB, and 20 dB. These reductions turn out to be lower than those for $D = 2$. It is a consequence of the spatial diversity achieved by using multiple antennas at the transmitter/receiver.

We now study the effect of the number of subcarriers and $f_d\tau$ on the throughput in Fig. 8. We consider the independent subcarrier scenario with $N_{sc} = 1, 12$, and 24 since this was the more challenging case for the proposed bivariate EESM model. We see that as the feedback delay increases, the throughput decreases more rapidly for $N_{sc} = 1$ (narrowband case) than for $N_{sc} = 24$. This is a consequence of the frequency diversity achieved by transmitting over multiple subcarriers.

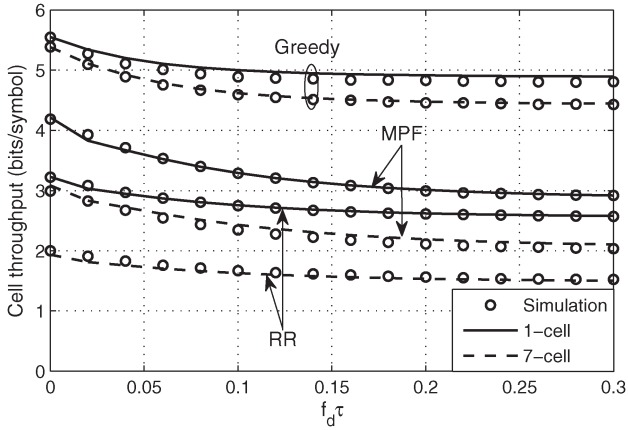


Fig. 9. Independent subcarriers: Cell throughput as a function of normalized delay for different schedulers with and without co-channel interference (Cell corner SNR = 5 dB, $K = 10$, $N_{sc} = 24$, and $D = 2$ (SISO)).

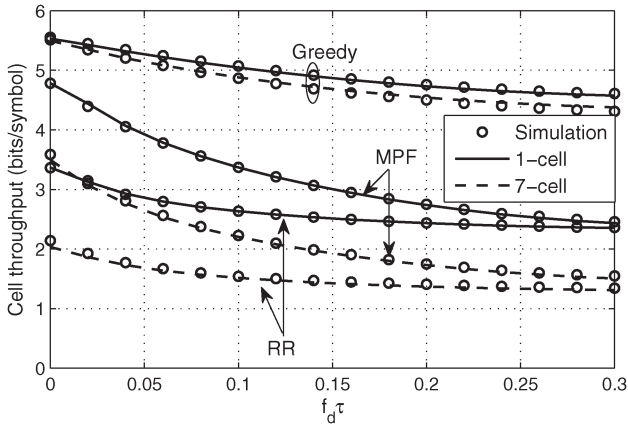


Fig. 10. RA channel: Cell throughput as a function of normalized delay for different schedulers with and without co-channel interference (Cell corner SNR = 5 dB, $K = 10$, $N_{sc} = 24$, and $D = 2$ (SISO)).

B. Multi-Cell, Multi-User Scenario

We consider a hexagonal cellular layout with $M = 6$ first-tier BSs as the co-channel interfering cells. The cell radius is $R = 10d_0$ and the number of users in a cell is $K = 10$. The k th user is located at a distance of Rk/K from the BS and at an azimuth of $2\pi k/K$. Such a user placement makes the channels at different locations in the cell from the serving and interfering BSs statistically heterogeneous. We set $N_{sc} = 24$, $\sigma_{shad} = 8$ dB, $\eta = 3.7$, and $P_S/P_N = 42$ dB, which corresponds to a cell corner SNR of 5 dB.

Figs. 9 and 10 plot the cell throughput against $f_d\tau$ for independent subcarriers and for the RA channel, respectively. Notice the good match between the analysis and the simulation results in both figures. This verifies the accuracy of the proposed mixture model as well as the cell throughput analysis. For independent subcarriers with greedy, RR, and MPF schedulers, the cell throughput respectively decreases by 14%, 20%, and 31% in the single-cell scenario, and by 18%, 24%, and 33% in the multi-cell scenario, when $f_d\tau$ increases from 0 to 0.3. Similar trends arise in the RA channel as well. We see that for all the schedulers, the drop in throughput is higher in the presence of co-channel interference.

The greedy scheduler has the least drop in throughput because it schedules users closer to the BS, which often report the higher rate MCSs. This minimizes the loss due to underestimation or overestimation of the MCSs. The RR scheduler's throughput is also relatively less sensitive to feedback delays because it does not use channel state information for scheduling. The MPF scheduler suffers the most for the following reason. It typically schedules a user when its reported rate is much higher than its fading-averaged value. However, the channel gain is most likely to fall after these time instances [24], which increases the odds of an outage.

V. CONCLUSION

We presented a general analytical framework to characterize the impact of feedback delay on EESM-based wideband link adaptation in OFDM systems that operate over frequency-selective channels. In the process, we also developed an accurate statistical model for the time evolution of effective SNR. We proposed a novel bivariate gamma distribution for it in a point-to-point scenario and generalized it to a novel bivariate gamma mixture distribution in a multi-cell, multi-user scenario. These models apply to different multiple antenna diversity modes and different schedulers.

We saw that the throughput was more sensitive to feedback delays for less dispersive multipath channels and for lower diversity multiple antenna modes. Further, the cell throughput degradation due to feedback delays depended on the scheduler. The MPF scheduler suffered the most degradation as the odds of an outage were higher for it. An interesting avenue for future work is considering power adaptation in addition to rate adaptation and scheduling to maximize the throughput or the energy efficiency of the system.

APPENDIX A

PROBABILITY OF SUCCESSFUL TRANSMISSION WITH MCS m

We simplify the expression for the probability of successful transmission with MCS m in (3) by dropping some of the events and, thus, replacing it with its upper bound:

$$P(m_{\text{opt}}(t) = m) \approx P\left(\gamma_{\text{eff}}^{(m)}(t) \geq T_m, \gamma_{\text{eff}}^{(m+1)}(t) < T_{m+1}, \gamma_{\text{eff}}^{(m)}(t + \tau) \geq T_m\right). \quad (31)$$

Notice that the expression in (31) still requires the joint distribution of $\gamma_{\text{eff}}^{(m)}(t)$, $\gamma_{\text{eff}}^{(m+1)}(t)$, and $\gamma_{\text{eff}}^{(m)}(t + \tau)$, whose closed-form is unknown. We circumvent this challenge as follows. Using the law of total probability, we get

$$\begin{aligned} & P\left(\gamma_{\text{eff}}^{(m)}(t) \geq T_m, \gamma_{\text{eff}}^{(m+1)}(t) < T_{m+1}, \gamma_{\text{eff}}^{(m)}(t + \tau) \geq T_m\right) \\ &= P\left(\gamma_{\text{eff}}^{(m)}(t) \geq T_m, \gamma_{\text{eff}}^{(m)}(t + \tau) \geq T_m\right) \\ &\quad - P\left(\gamma_{\text{eff}}^{(m)}(t) \geq T_m, \gamma_{\text{eff}}^{(m+1)}(t) \geq T_{m+1}, \gamma_{\text{eff}}^{(m)}(t + \tau) \geq T_m\right). \end{aligned} \quad (32)$$

Then, the probability $P(\gamma_{\text{eff}}^{(m)}(t) \geq T_m, \gamma_{\text{eff}}^{(m+1)}(t) \geq T_{m+1}, \gamma_{\text{eff}}^{(m)}(t + \tau) \geq T_m)$ in (32) is replaced with the upper bound $P(\gamma_{\text{eff}}^{(m+1)}(t) \geq T_{m+1}, \gamma_{\text{eff}}^{(m)}(t + \tau) \geq T_m)$. The resulting expression is then substituted in (31) to yield (4).

APPENDIX B

BRIEF DERIVATION OF MOMENTS OF

$Y_{m_1}(t)$ AND $Y_{m_2}(t + \tau)$

The means of $Y_{m_1}(t)$ and $Y_{m_2}(t + \tau)$ are derived in [18], and are not shown here. Here, we derive the cross-correlation between $Y_{m_1}(t)$ and $Y_{m_2}(t + \tau)$ and the second moment. The cross-correlation is given by

$$\begin{aligned} \mathbb{E}[Y_{m_1}(t)Y_{m_2}(t + \tau)] &= \frac{1}{N_{\text{sc}}^2} \sum_{i=1}^{N_{\text{sc}}} \sum_{j=1}^{N_{\text{sc}}} \mathbb{E} \left[e^{\left(-\frac{\gamma_i(t)}{\beta_{m_1}} - \frac{\gamma_j(t+\tau)}{\beta_{m_2}} \right)} \right], \quad (33) \end{aligned}$$

$$= \frac{1}{N_{\text{sc}}^2} \sum_{i=1}^{N_{\text{sc}}} \sum_{j=1}^{N_{\text{sc}}} \Psi_{\gamma_i(t), \gamma_j(t+\tau)}(\beta_{m_1}^{-1}, \beta_{m_2}^{-1}). \quad (34)$$

The joint MGF of $\gamma_i(t)$ and $\gamma_j(t + \tau)$ is given by (8) with $q = D/2$, $s = 2a$, $p = 2a$, and $r = 4a^2(1 - \rho(\tau)|C_{ij}|^2)$, which when substituted in (34) yields (18). Substituting $\tau = 0$ in (18) yields the expression for the second moment in (17).

APPENDIX C

MGF OF $\Omega_k^{(n)}(t)$

The MGF $\Psi_{\Omega_k^{(n)}(t)}(z)$ of $\Omega_k^{(n)}(t)$ is given by $\Omega_k^{(n)}(t)(z) = \mathbb{E} \left[\exp \left(-z \left\{ \sum_{j=1}^M \frac{P_S}{P_N} \alpha_{jk} |h_{11}^{(n,k,j)}(t)|^2 + 1 \right\} \right) \right]$. Since the channel gains of interfering links from different BSs are independent, we get $\Psi_{\Omega_k^{(n)}(t)}(z) = \exp(-z) \prod_{j=1}^M \Psi_j(z)$, where $\Psi_j(z) = \mathbb{E} \left[\exp \left(-z \frac{P_S}{P_N} \alpha_{jk} |h_{11}^{(n,k,j)}(t)|^2 \right) \right]$ and is evaluated as follows. Averaging over the lognormal RV α_{jk} , we get

$$\Psi_j(z) = \int_0^\infty \mathbb{E} \left[e^{-z \frac{P_S}{P_N} \alpha} |h_{11}^{(n,k,j)}(t)|^2 \right] e^{-\frac{(\log(\alpha) - \mu_{jk})^2}{2\sigma_{\text{shad}}^2}} \frac{d\alpha}{\sqrt{2\pi}\sigma_{\text{shad}}\alpha}. \quad (35)$$

The RV $|h_{11}^{(n,k,j)}(t)|^2$ is exponentially distributed. Therefore, $\mathbb{E} \left[\exp \left(-z \frac{P_S}{P_N} \alpha |h_{11}^{(n,k,j)}(t)|^2 \right) \right] = \left(1 + z \frac{P_S}{P_N} \alpha \right)^{-1}$. Using the variable substitution $\omega = \frac{\log(\alpha) - \mu_{jk}}{\sqrt{2}\sigma_{\text{shad}}}$ in (35) followed by Gauss-Hermite quadrature, we get

$$\Psi_j(z) \approx \sum_{i=1}^{N_{GH}} \frac{w_i}{\sqrt{\pi}} \left(1 + z \frac{P_S}{P_N} e^{\mu_{jk} + \sqrt{2}\sigma_{\text{shad}}\lambda_i} \right)^{-1}. \quad (36)$$

Substituting (36) in $\Psi_{\Omega_k^{(n)}(t)}(z)$ yields (22).

APPENDIX D

EVALUATING $P(S_t = k | R_k(t) = r_m)$

1) *RR Scheduler*: Since the users are scheduled periodically, the selected user does not depend on $R_k(t)$. Thus, $P(S_t = k | R_k(t) = r_m) = P(S_t = k) = 1/K$.

2) *Greedy Scheduler*: Let $\{\Lambda(t) = r_m\}$ denote the event that all the users in the set $\Lambda(t)$ report rate r_m at time t . Let $|\Lambda(t)|$ denote the cardinality of the set $\Lambda(t)$, and let $\Lambda^c(t)$ denote its complement. If v other users along with user k report the same highest rate, for $0 \leq v \leq K - 1$, then user k is selected with probability $1/(v + 1)$. From the law of total probability, we get

$$\begin{aligned} P(S_t = k | R_k(t) = r_m) &= \sum_{v=1}^{K-1} \frac{1}{v+1} \sum_{\substack{\Lambda(t) \subset \{1, \dots, K\} \\ |\Lambda(t)| = v}} \times P(R_{\Lambda(t)} = r_m, R_{\Lambda^c(t) \setminus \{k\}} < r_m | R_k(t) = r_m) \\ &\quad + P(R_g(t) < R_k(t), \forall g \neq k | R_k(t) = r_m). \quad (37) \end{aligned}$$

Since the rates reported by the users are independent, we get

$$\begin{aligned} P(S_t = k | R_k(t) = r_m) &= \sum_{v=1}^{K-1} \frac{1}{v+1} \sum_{\substack{n_1=1 \\ n_1 \neq k}}^K \dots \sum_{\substack{n_v = n_{v-1} + 1 \\ n_v \neq k}}^K \prod_{g \in \{n_1, \dots, n_v\}} P(R_g(t) = r_m) \\ &\quad \times \prod_{\substack{h=1 \\ h \notin \{k, n_1, \dots, n_v\}}}^K P(R_h(t) < r_m) + \prod_{\substack{g=1 \\ g \neq k}}^K P(R_g(t) < r_m). \quad (38) \end{aligned}$$

Using the bivariate gamma mixture model for EESM in (25), the probability that user k reports rate r_m is given by

$$\begin{aligned} P(R_k(t) = r_m) &= \begin{cases} \sum_{i=1}^{N_{GH}} \tilde{w}_i \Gamma_{\text{inc}} \left(q_{1,1}^{(k,i)}, \frac{T_1}{s_{1,1}^{(k,i)}} \right), & m = 0, \\ \sum_{i=1}^{N_{GH}} \tilde{w}_i \left[\Gamma_{\text{inc}} \left(q_{m+1,m}^{(k,i)}, \frac{T_{m+1}}{s_{m+1,m}^{(k,i)}} \right) \right. \\ \quad \left. - \Gamma_{\text{inc}} \left(q_{m,m}^{(k,i)}, \frac{T_m}{s_{m,m}^{(k,i)}} \right) \right], & 1 \leq m \leq L. \end{cases} \quad (39) \end{aligned}$$

Substituting (39) in (38) yields the desired expression in (28).

3) *MPF Scheduler*: User k is scheduled if it has the highest ratio of the rate reported to its average rate. Since this ratio is a real number, ties between users occur with zero probability and need not be considered. Thus,

$$\begin{aligned} P(S_t = k | R_k(t) = r_m) &= P \left(\frac{R_g(t)}{\mathbb{E}R_g(t)} < \frac{R_k(t)}{\mathbb{E}R_k(t)}, \forall g \neq k | R_k(t) = r_m \right). \quad (40) \end{aligned}$$

Since the rates reported by the users are independent, we get $P(S_t = k | R_k(t) = r_m) = \prod_{\substack{g=1 \\ g \neq k}}^K P(R_g(t) < r_{m_{gk}})$, where m_{gk} is defined in the result statement. Evaluating these probabilities using (39) yields the desired expression in (29).

REFERENCES

- [1] J. Francis and N. B. Mehta, "Impact of feedback delays on EESM-based wideband link adaptation: Modeling and analysis," in *Proc. IEEE GLOBECOM*, Austin, TX, USA, Dec. 2014, to be published.
- [2] S. Sesia, I. Toufik, and M. Baker, *LTE—The UMTS Long Term Evolution, From Theory to Practice*, 1st ed. Hoboken, NJ, USA: Wiley, 2009.
- [3] A. J. Goldsmith, *Wireless Communications*, 1st ed. Cambridge, U.K.: Cambridge Univ. Press, 2005.
- [4] T. L. Jensen, S. Kant, J. Wehinger, and B. H. Fleury, "Fast link adaptation for MIMO OFDM," *IEEE Trans. Veh. Technol.*, vol. 59, no. 8, pp. 3766–3778, Oct. 2010.
- [5] K. Brueninghaus *et al.*, "Link performance models for system level simulations of broadband radio access systems," in *Proc. IEEE PIMRC*, Sep. 2005, pp. 2306–2311.
- [6] S. S. Tsai and A. C. K. Soong, "Effective-SNR mapping for modeling frame error rates in multiple-state channels," Third Generation Partnership Project 2 (3GPP2), Arlington, VA, USA, Tech. Rep. 3GPP2-C30-20030429-010, 2003.
- [7] "Feasibility study for OFDM for UTRAN enhancement," 3rd Generation Partnership Project (3GPP), Sophia Antipolis, France, Tech. Rep. 25.892 v2.0.0 (2004-06), 2004.
- [8] R. Srinivasan, J. Zhuang, L. Jalloul, R. Novak, and J. Park, "IEEE 802.16m evaluation methodology document (EMD)," Tech. Rep. IEEE 802.16m-08/004r2, 2008.
- [9] S. N. Donthi and N. B. Mehta, "An accurate model for EESM and its application to analysis of CQI feedback schemes and scheduling in LTE," *IEEE Trans. Wireless Commun.*, vol. 10, no. 10, pp. 3436–3448, Oct. 2011.
- [10] A. Kuhne and A. Klein, "Throughput analysis of multi-user OFDMA-systems using imperfect CQI feedback and diversity techniques," *IEEE J. Sel. Areas Commun.*, vol. 26, no. 8, pp. 1440–1450, Oct. 2008.
- [11] S. Ye, R. S. Blum, and L. J. Cimini, "Adaptive OFDM systems with imperfect channel state information," *IEEE Trans. Wireless Commun.*, vol. 5, no. 11, pp. 3255–3265, Nov. 2006.
- [12] M. Goldenbaum, R. A. Akl, S. Valentin, and S. Stanczak, "On the effect of feedback delay in the downlink of multiuser OFDM systems," in *Proc. CISS*, Mar. 2011, pp. 1–6.
- [13] S. Guharoy and N. B. Mehta, "Joint evaluation of channel feedback schemes, rate adaptation, scheduling in OFDMA downlinks with feedback delays," *IEEE Trans. Veh. Technol.*, vol. 62, no. 4, pp. 1719–1731, May 2013.
- [14] Y. Huang and B. D. Rao, "Performance analysis of heterogeneous feedback design in an OFDMA downlink with partial and imperfect feedback," *IEEE Trans. Signal Process.*, vol. 61, no. 4, pp. 1033–1046, Feb. 2013.
- [15] V. Annapureddy, D. Marathe, T. R. Ramya, and S. Bhashyam, "Outage probability of Multiple-Input Single-Output (MISO) systems with delayed feedback," *IEEE Trans. Commun.*, vol. 57, no. 2, pp. 319–326, Feb. 2009.
- [16] S. Simoens, S. Rouquette-Léveil, P. Sartori, Y. Blankenship, and B. Classon, "Error prediction for adaptive modulation and coding in multiple-antenna OFDM systems," *Signal Process.*, vol. 86, no. 8, pp. 1911–1919, Aug. 2006.
- [17] T. Tao and A. Czulwik, "Performance analysis of link adaptation in LTE systems," in *Proc. Int. ITG WSA*, Feb. 2011, pp. 1–5.
- [18] J. Francis and N. B. Mehta, "EESM-based link adaptation in point-to-point and multi-cell OFDM systems modeling and analysis," *IEEE Trans. Wireless Commun.*, vol. 13, no. 1, pp. 407–417, Jan. 2014.
- [19] F. Chatelain, J.-Y. Tournet, J. Inglada, and A. Ferrari, "Bivariate gamma distributions for image registration and change detection," *IEEE Trans. Image Process.*, vol. 16, no. 7, pp. 1796–1806, Jul. 2007.
- [20] H. Song, R. Kwan, and J. Zhang, "Approximations of EESM effective SNR distribution," *IEEE Trans. Commun.*, vol. 59, no. 2, pp. 603–612, Feb. 2011.
- [21] N. B. Mehta, J. Wu, A. F. Molisch, and J. Zhang, "Approximating a sum of random variables with a lognormal," *IEEE Trans. Wireless Commun.*, vol. 6, no. 7, pp. 2690–2699, Jul. 2007.
- [22] J.-G. Choi and S. Bahk, "Cell-throughput analysis of the proportional fair scheduler in the single-cell environment," *IEEE Trans. Veh. Technol.*, vol. 56, no. 2, pp. 766–778, Mar. 2007.
- [23] J. Fan, Q. Yin, G. Y. Li, B. Peng, and X. Zhu, "MCS selection for throughput improvement in downlink LTE systems," in *Proc. ICCCN*, Aug. 2011, pp. 1–5.
- [24] G. L. Stuber, *Principles of Mobile Communications*. Boston, MA, USA: Kluwer, 1996.
- [25] I. S. Gradshteyn and I. M. Ryzhik, *Table of Integrals, Series and Products*, 4th ed. San Diego, CA, USA: Academic, 1980.
- [26] Y. Li, L. Zhang, L. J. Cimini, and H. Zhang, "Statistical analysis of MIMO beamforming with co-channel unequal-power MIMO interferers under path-loss and rayleigh fading," *IEEE Trans. Signal Process.*, vol. 59, no. 8, pp. 3738–3748, Aug. 2011.
- [27] "Universal mobile telecommunications system (UMTS); deployment aspects," 3rd Generation Partnership Project (3GPP), Sophia Antipolis, France, Tech. Rep. 25943 v6.0.0 (2004-12), 2004.
- [28] T. M. Cover and J. A. Thomas, *Elements of Information Theory*. Hoboken, NJ, USA: Wiley, 1991, ser. Wiley series in telecommunications.
- [29] F. Perez-Cruz, "Kullback-leibler divergence estimation of continuous distributions," in *Proc. IEEE ISIT*, Jul. 2008, pp. 1666–1670.
- [30] M. Abramowitz and I. Stegun, *Handbook of Mathematical Functions with Formulas, Graphs, Mathematical Tables*, 9th ed. New York, NY, USA: Dover, 1972.
- [31] S. Atapattu, C. Tellambura, and H. Jiang, "Representation of composite fading and shadowing distributions by using mixtures of gamma distributions," in *Proc. IEEE WCNC*, Apr. 2010, pp. 1–5.
- [32] A. Jalali, R. Padovani, and R. Pankaj, "Data throughput of CDMA-HDR a high efficiency-high data rate personal communication wireless system," in *Proc. IEEE VTC—Spring*, May 2000, pp. 1854–1858.



Jobin Francis received the B.Tech. degree in electronics and communication engineering from the College of Engineering, Trivandrum, India, in 2009, the M.Eng. degree in signal processing from the Indian Institute of Science (IISc), Bangalore, India, in 2011. He is currently pursuing the Ph.D. degree with the Department of Electrical Communication Engineering, IISc. His research interests include design and analysis of link adaptation in next generation cellular systems and resource allocation in wireless networks.



Neelesh B. Mehta (S'98–M'01–SM'06) received the B.Tech. degree in electronics and communications engineering from the Indian Institute of Technology (IIT), Madras, India, in 1996, and the M.S. and Ph.D. degrees in electrical engineering from the California Institute of Technology, Pasadena, CA, USA, in 1997 and 2001, respectively. He is now an Associate Professor in the Department of Electrical Communication Eng., Indian Institute of Science (IISc), Bangalore. He serves as an Executive Editor of IEEE TRANSACTIONS ON WIRELESS COMMUNICATION and as an Editor of IEEE TRANSACTIONS ON COMMUNICATIONS and IEEE WIRELESS COMMUNICATION LETTERS. He currently serves as a Member-at-Large on the Board of Governors of IEEE COMSoc.